

A Law of Data Separation in Deep Learning

Hangfeng He*

Weijie J. Su†

October 30, 2022

Abstract

Multilayer neural networks have achieved superhuman performance in many artificial intelligence applications. However, their black-box nature obscures the underlying mechanism for transforming input data into labels throughout all layers, thus hindering architecture design for new tasks and interpretation for high-stakes decision makings. We addressed this problem by introducing a precise law that governs how real-world deep neural networks separate data according to their class membership from the bottom layers to the top layers in classification problems. This law shows that each layer roughly improves a certain measure of data separation by an *equal* multiplicative factor. This law manifests in modern architectures such as AlexNet, VGGNet, and ResNet in the late phase of training. This law together with the perspective of data separation offers practical guidelines for designing network architectures, improving model robustness and out-of-sample performance during training, as well as interpreting deep learning predictions.

Deep learning methodologies have achieved remarkable success across a wide range of data-intensive tasks [21, 23, 27, 7]. In contrast to other machine learning techniques [9], however, the practice of deep learning relies heavily on a plethora of heuristics and tricks that are not well justified. This situation often makes deep learning-based approaches ungrounded for some applications or necessitates the need for huge computational resources for exhaustive search [16], making it difficult to fully realize the potential of this set of methodologies.

This unfortunate situation is in part owing to a lack of understanding of how the prediction depends on the interior layers of deep neural networks [1, 24, 6]. In particular, little is known about how the data of different classes (e.g., images of cats and dogs) in classification problems are gradually separated from the bottom layers to the top layers in modern architectures such as AlexNet [21] and residual neural networks [12]. Any knowledge about data separation, especially quantitative characterization, would offer useful principles and insights for designing network architectures, training processes, and model interpretation.

The main finding of this paper is a quantitative and precise delineation of the data separation process throughout all layers of real-world deep neural networks. As an illustration, Figure 1 plots a certain value that measures how well the data are separated according to their class membership in each layer in a neural network trained on the Fashion-MNIST dataset [36]. This value in the logarithmic scale decays, in a distinct manner, linearly in the number of layers the data have passed through. Indeed, the Pearson correlation coefficients between the logarithm of this value and the layer index range from -0.997 and -1 in Figure 1. This phenomenon is unexpected because there is no explicit constraint during training that forces this exponential decay.

*University of Rochester. Email: hangfeng.he@rochester.edu.

†University of Pennsylvania. Email: suw@wharton.upenn.edu.

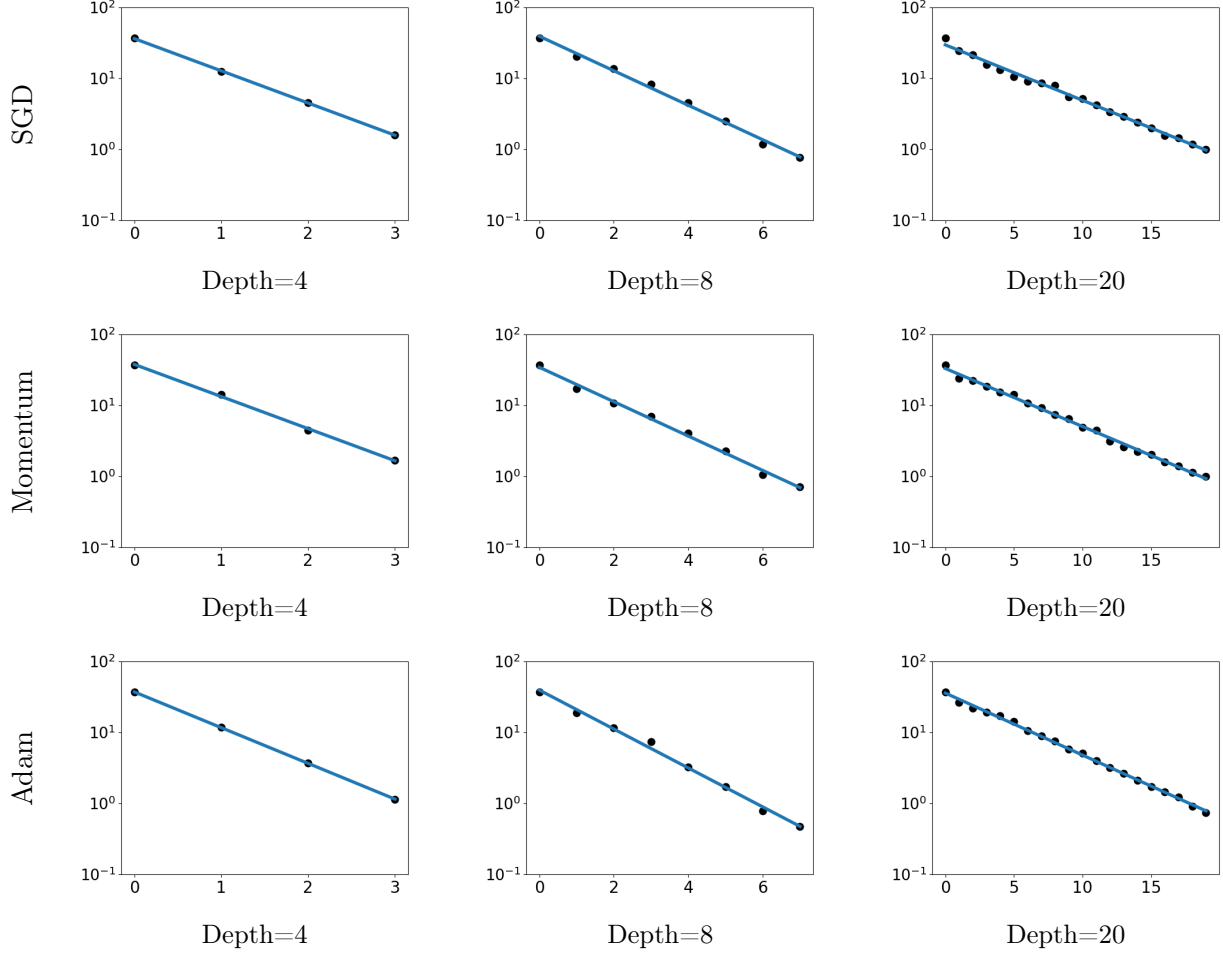


Figure 1: Illustration of the law of equi-separation in feedforward neural networks with ReLU activations trained on the Fashion-MNIST dataset. The three columns correspond to depths of 4, 8, and 20, and the three rows correspond to the training methods stochastic gradient descent (SGD), SGD with momentum, and Adam. Throughout the paper, the x axis represents the layer index and the y axis represents the separation fuzziness (1), unless otherwise specified. The Pearson correlation coefficients, by row first, are -1.000 , -0.998 , -0.997 , -0.999 , -0.998 , -0.998 , -1.000 , -0.997 , and -0.999 . More details can be found in Appendix A.

The measure shown in Figure 1 is canonical for measuring data separation in classification problems. Let x_{ki} denote an intermediate output of a neural network on the i th point of Class k for $1 \leq i \leq n_k$, $\bar{x}_k := (x_{k1} + \dots + x_{kn_k})/n_k$ denote the sample mean of Class k , and $\bar{x} := (n_1\bar{x}_1 + \dots + n_K\bar{x}_K)/n$ denote the global mean, where $n := n_1 + \dots + n_K$. We define the between-class sum of squares and the within-class sum of squares as

$$\text{SS}_b := \frac{1}{n} \sum_{k=1}^K n_k (\bar{x}_k - \bar{x})(\bar{x}_k - \bar{x})^\top \quad \text{and} \quad \text{SS}_w := \frac{1}{n} \sum_{k=1}^K \sum_{i=1}^{n_k} (x_{ki} - \bar{x}_k)(x_{ki} - \bar{x}_k)^\top,$$

respectively. The former matrix represents the between-class “signal” for classification, whereas the latter denotes the within-class variability. Writing SS_b^+ for the Moore–Penrose inverse of SS_b ,¹ the ratio matrix $\text{SS}_w \text{SS}_b^+$ can be thought of as the inverse signal-to-noise ratio. We use its trace

$$D := \text{Tr}(\text{SS}_w \text{SS}_b^+) \tag{1}$$

to measure how well the data are separated [31, 25]. This value, which is referred to as the separation fuzziness, is large when the data points are not concentrated to their class means or, equivalently, are not well separated, and vice versa. A large value of separation fuzziness limits the classification accuracy using the present data. On the other hand, if all points are all collapsed to their class means, the separation fuzziness equals zero.

Given an L -layer neural network, let D_l denote the separation fuzziness (1) of the training data passing through the first l layers for $0 \leq l \leq L - 1$.² Figure 1 suggests that the dynamics of D_l follows the relation

$$D_l \doteq \rho^l D_0$$

for some decay ratio $0 < \rho < 1$. Alternatively, this law implies $\log D_{l+1} - \log D_l \doteq -\log \frac{1}{\rho}$, showing that the neural network makes equal progress in reducing $\log D$ over each layer on the training data. Hence, we call this the *law of equi-separation*. The decay ratio ρ depends on the depth of the neural network, dataset, training time, and network architecture, and is also affected, to a lesser extent, by optimization methods and many other hyperparameters. For the 20-layer network trained using Adam [19] (the bottom-right plot of Figure 1), the decay ratio ρ is 0.818. Thus, the half-life is $\frac{\ln 2}{\ln \rho^{-1}} = \frac{0.693}{\ln \rho^{-1}} = 3.45$, suggesting that this 20-layer neural network reduces the value of the separation fuzziness in every three and a half layers.

The law of equi-separation is pervasive as it continues to hold irrespective of datasets and network architectures, and it persists for different values of learning rate and various levels of imbalance between classes, as shown in Figure 2. Furthermore, Figure 8 in the Appendix shows that the law also holds in a more fine-grained class-wise manner. The nonlinearity of neural networks is vital to this law because the separation fuzziness is roughly invariant under linear transformations. In addition, this law is not implied by analyses of neural networks using neural tangent kernel [18]. This approach is not capable of capturing the effect of depth, which is critical for understanding the data separation process throughout all layers.

This phenomenon manifests in the terminal phase of training [25], where we continue to train the model to interpolate in-sample data. At the beginning of the training, the bottom layers start

¹The matrix SS_b has rank at most $K - 1$ and is not invertible in general since the dimension of the data is typically larger than the number of classes.

²For clarification, D_0 is calculated from the raw data, and D_1 is calculated from the data that have passed through the first layer but not the second layer.

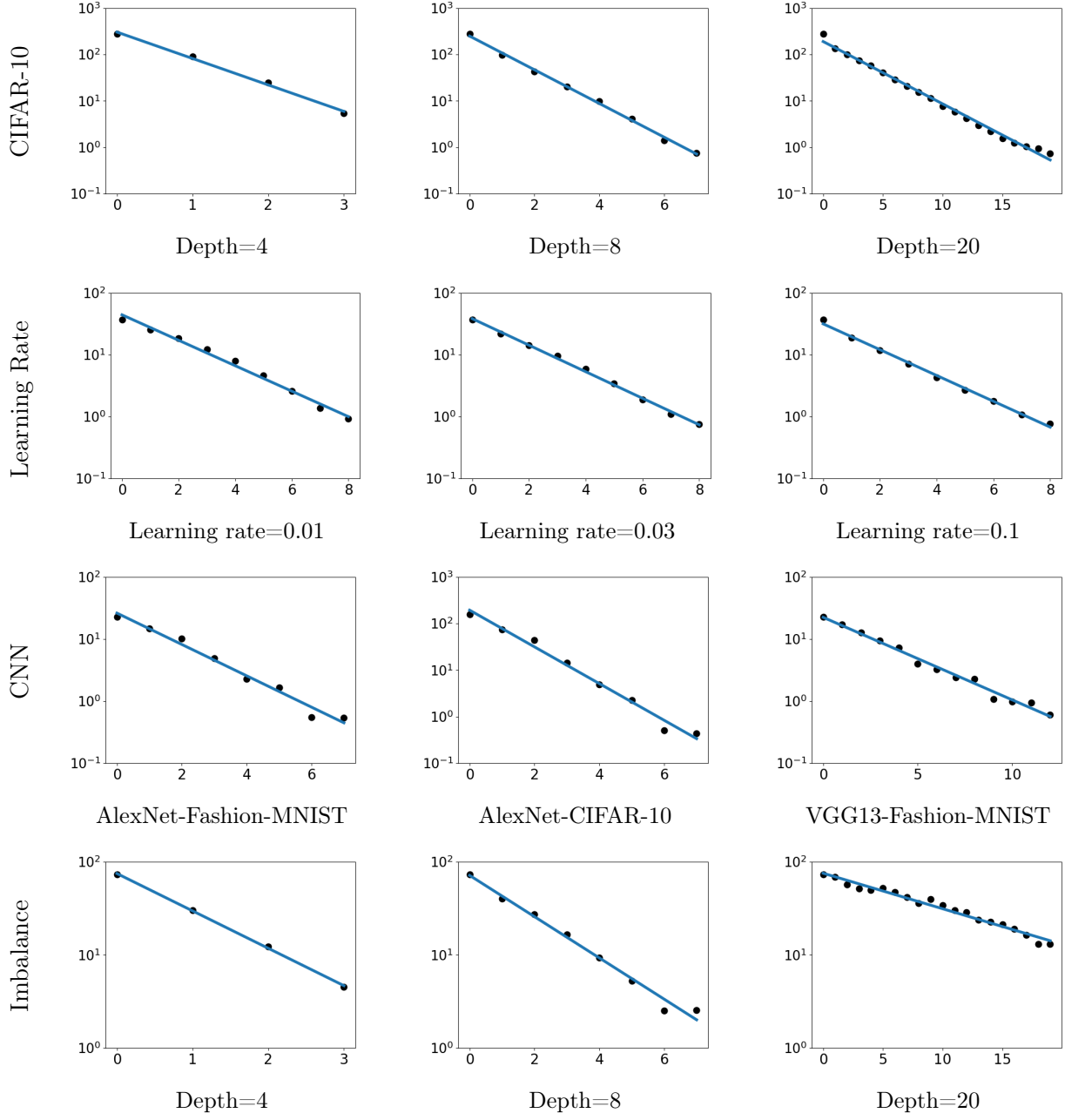


Figure 2: Illustration showing how the law of equi-separation holds in a wide range of settings. The second and fourth rows use Fashion-MNIST. Details of the experimental settings are given in Appendix A.

to learn to reduce the separation fuzziness faster than the top layers can (see Figure 10 in the Appendix), whereas at later stages, the top layers catch up as the bottom layers have learned the features. Remarkably, each layer finally becomes roughly equal in reducing the separation fuzziness multiplicatively during training. Neural networks in the terminal phase of training also exhibit certain symmetric geometries in the last layer such as neural collapse [25] and minority collapse [6]. The law of equi-separation emerges earlier than these two empirical patterns during training. More importantly, the law delineates the entire data separation process, whereas neural collapse and minority collapse capture only the endpoint of the process.

A perspective informed by this law is to focus on the non-temporal dynamics of the data separation process throughout all layers when studying deep neural networks. This perspective probes into the interior of deep learning models by perceiving the black-box classifier as a sequence of transformations, each of which corresponds to a layer. In contrast, existing analyses often consider the “exterior” of these models by focusing on the loss function or test performance, without considering the interior layers [18, 10, 2]. Owing to its preciseness and simplicity, the law of equi-separation together with this new perspective may be able to offer an effective approach for guiding deep learning practice. Indeed, in the remainder of this paper, we show how it would benefit the three basic components of deep learning practice, namely, architecture design, training, and interpretation.

Network architecture. The law of equi-separation can inform the design principles for network architecture. First, the law implies that neural networks should be deep for good performance, thereby reflecting the hierarchical nature of deep learning [3, 23, 26, 13]. This is because, taken together, all layers reduce the separation fuzziness D_0 of the raw input to $\rho^{L-1}D_0$ at the last layer. When the depth L is large, the ratio ρ^{L-1} is exponentially small even when ρ is close to 1—meaning each layer improves separation only a bit. In contrast, when L is small—say, $L = 2$ or 3—the ratio ρ^{L-1} would generally not be small and, therefore, the neural network is unlikely to separate the data well. In the literature, the fundamental role of depth is recognized by analyzing the loss functions [3, 12, 8, 37, 28], and our law of equi-separation offers a new perspective on depth.

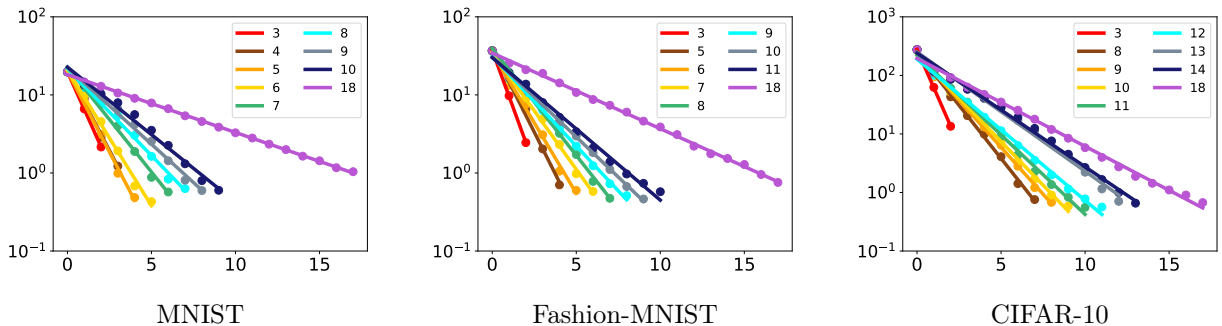


Figure 3: Illustration of the law of equi-separation with varying network depths. The legend shows how depths are color coded. The optimal depth that yields the lowest separation fuzziness depends on the dataset complexity.

For completeness, the deeper the better is not necessarily true in practice because a very large depth would render the optimization problem challenging. As shown in Figure 1, the 20-layer neural networks have higher values of the final separation fuzziness than those of their 8-layer counterparts.

The Fashion-MNIST dataset is not very complex and, therefore, an 8-layer network will suffice to classify the data well. Adding additional layers, therefore, would only give rise to optimization burdens. Indeed, Figure 3 illustrates the law of equi-separation with varying network depths, showing that different datasets correspond to different optimal depths. Therefore, as a practical guideline, the choice of depth should consider the complexity of the applications. For instance, this perspective of data separation shows that the optimal depths for MNIST [22], Fashion-MNIST, and CIFAR-10 [20] are 6, 10, and 12, respectively. This is consistent with the increasing complexity from MNIST to Fashion-MNIST to CIFAR-10 [11, 30, 12].

Moreover, the law of equi-separation implies that depth is more crucial than the “shape” of neural networks. In the first row of Figure 4, the network does not separate the data well when the width of each layer is merely 20. This is because the network has to be wide enough to pass the useful features of the data for classification. However, when the network is wide enough, the network performance may be saturated even if more neurons are added to each layer. For example, the equi-separation law has about the same final value of separation fuzziness for both widths of 100 and 1000, although, in general, the saturation width may vary with respect to the datasets [15]. In addition, the second row of Figure 4 shows that it is better to start with relatively wide layers at the bottom layers followed by narrow top layers. Overall, these observations suggest that very wide neural networks in general should not be recommended as they consume more time for optimization. Apart from encoding purposes, the width should be set to about the same across all layers or be made larger for the bottom layers [11, 33].

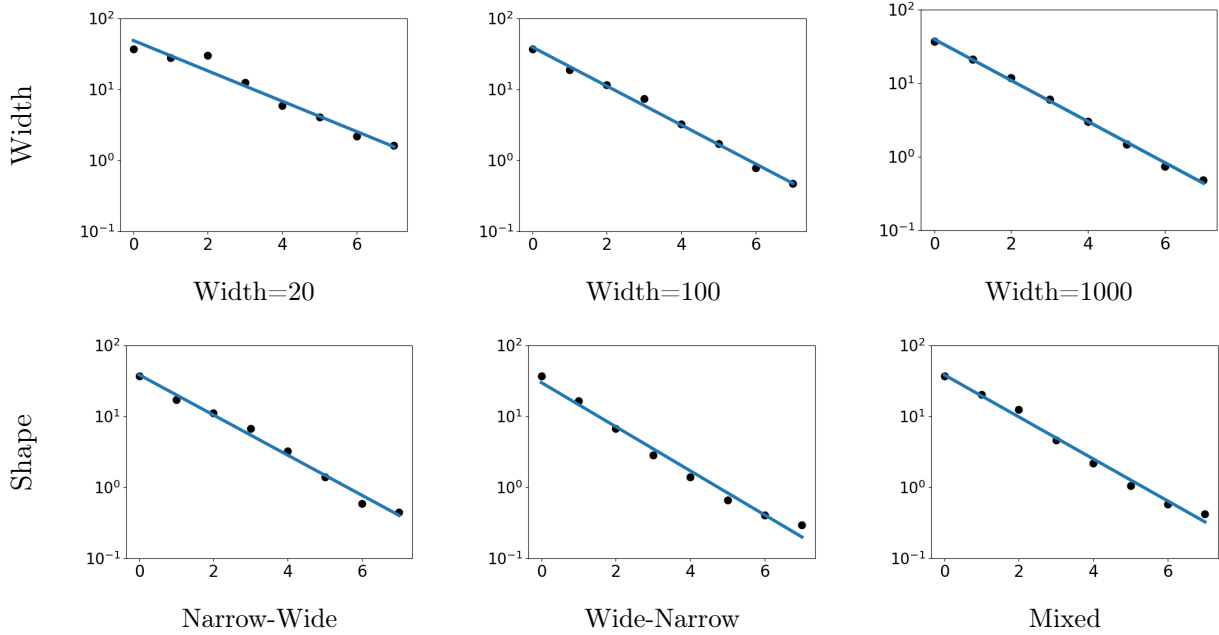


Figure 4: Illustration of the law of equi-separation with different widths and shapes of the neural networks. For example, “Narrow-Wide” means that the bottom layers are narrower than the top layers. See more details in Appendix A.

Although the law of equi-separation can be observed in a range of vision tasks, it is not seen in language models such as BERT [5] (see Figure 14 in the Appendix). This is perhaps because

language models learn a sequence of token-level features instead of sentence-level features in each layer. It would be of interest to investigate whether the law of equi-separation could be leveraged to obtain better sentence-level features using a sequence of token-level features.

Training. The emergence of the law of equi-separation during training is indicative of good model performance. For example, its manifestation can improve the robustness to model shifts [14]. Let

$$R := \frac{D_t}{D_{t-1}} \times \frac{D_{t-1}}{D_{t-2}} \times \cdots \times \frac{D_1}{D_0} = \frac{D_t}{D_0}$$

denote the reduction ratio of the separation fuzziness made by the entire network. On the assumption that a perturbation of the network weights leads to a change of ϵ in the ratio for each layer, the perturbed reduction ratio becomes

$$\left(\frac{D_t}{D_{t-1}} + \epsilon\right) \left(\frac{D_{t-1}}{D_{t-2}} + \epsilon\right) \cdots \left(\frac{D_1}{D_0} + \epsilon\right) = R + R \left(\frac{D_{t-1}}{D_t} + \frac{D_{t-2}}{D_{t-1}} + \cdots + \frac{D_0}{D_1}\right) \epsilon + O(\epsilon^2).$$

The perturbation term $R \left(\frac{D_{t-1}}{D_t} + \frac{D_{t-2}}{D_{t-1}} + \cdots + \frac{D_0}{D_1}\right) \epsilon$ is minimized in absolute value when $\frac{D_t}{D_{t-1}} = \frac{D_{t-1}}{D_{t-2}} = \cdots = \frac{D_1}{D_0}$. This is precisely the case when the equi-separation law holds. Thus, the data separation ability of the classifier is not very sensitive to perturbations in network weights when the law manifests. Therefore, to improve the robustness, we need to train a neural network at least until the law of equi-separation comes into effect. In the literature, however, connections with robustness are often established through loss functions rather than data separation [4].

The law of equi-separation can also shed light on the out-of-sample performance of neural networks. Figure 5 considers two neural networks where one exhibits the law of equi-separation and the other does not. The results of our experiments showed that the former one has better test performance. Although this law is sometimes not observed in neural networks with good test performance, interestingly, one can fine-tune the parameters to reactivate the law with about the same or better test performance.

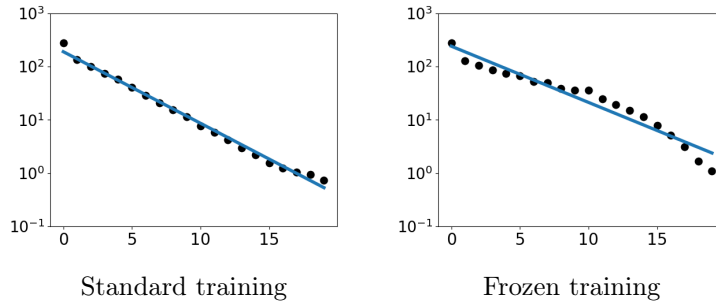


Figure 5: Illustration showing the law of equi-separation manifesting in the left network but not in the right network because of frozen training. Both networks have about the same training losses as well as training accuracies. However, the left network has a higher test accuracy (23.85%) than that of the right network (19.67%).

Moreover, the law of equi-separation can be potentially used to facilitate the training of transfer learning. In transfer learning, for example, bottom layers trained from an upstream task can form

part of a network that will be trained on a downstream task. A challenge arising in practice is how to balance between the training times on the source and the target. In light of the law of equi-separation, a sensible balance is to find when the improvement in reducing separation fuzziness is roughly the same between the bottom and top layers.

Interpretation. The equi-separation law offers a new perspective for interpreting deep learning predictions, especially in high-stakes decision makings. An important ingredient in interpretation is to pinpoint the basic operational modules in neural networks and subsequently to reflect that “all modules are created equal.” For feedforward and convolutional neural networks, each layer is a module as it reduces the separation fuzziness by an equal multiplicative factor (for more details, see Figure 13 in the Appendix). Interestingly, even when the law no longer manifests in residual neural networks, Figure 6 shows that it can be reactivated if a block rather than a layer is identified as a module. This figure also suggests that blocks containing more layers are more capable of reducing the separation fuzziness. For comparison, when the perspective of data separation is not considered [39], the correct module cannot be identified.

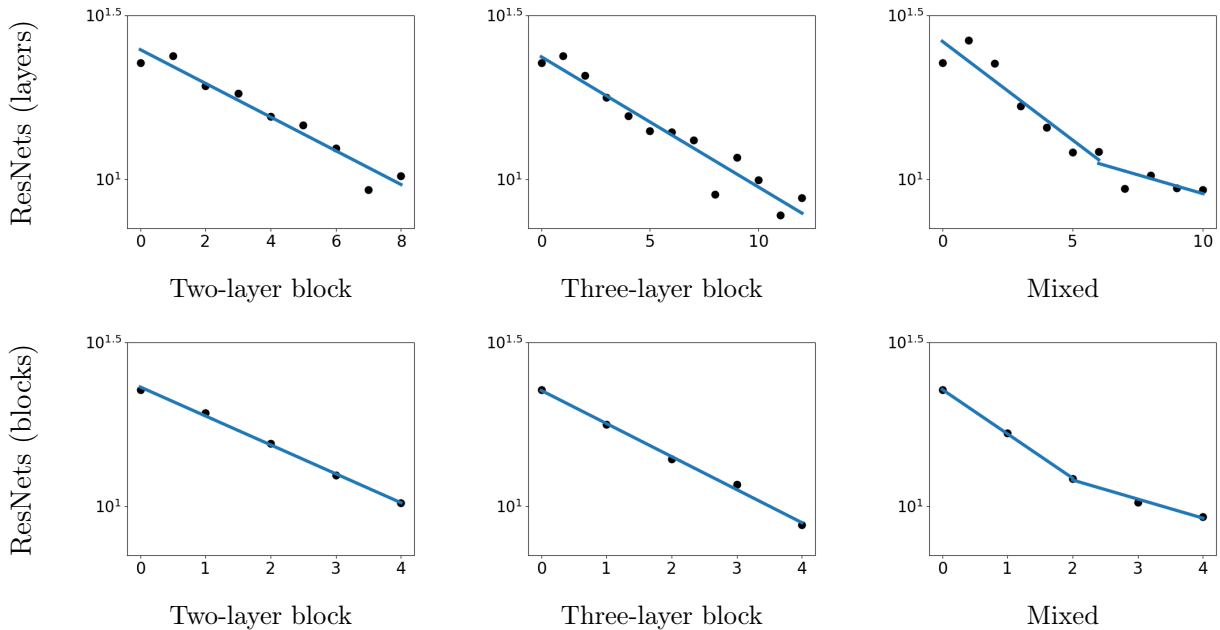


Figure 6: Illustration of the law of equi-separation in residual neural networks. Each block contains either 2 or 3 layers. For “Mixed”, the first two are 3-layer blocks, and the last two are 2-layer blocks. See more details in Appendix A.

Because each module makes equal but small contributions, a few neurons in a single layer are unlikely to explain how a deep learning model makes a particular prediction. It is therefore crucial to take all layers collectively for interpretation [32]. This view, however, challenges the layer-wise approaches to deep learning interpretation [38, 34]. Owing to the preciseness of the law of equi-separation, the perspective of data separation may offer formal insights into leveraging all layers for interpretation.

Acknowledgments

We would like to thank X.Y. Han for very helpful comments and feedback on an early version of the manuscript. This research was supported in part by NSF grants CCF-1934876 and CAREER DMS-1847415, and an Alfred Sloan Research Fellowship.

References

- [1] P. L. Bartlett, P. M. Long, G. Lugosi, and A. Tsigler. Benign overfitting in linear regression. *Proceedings of the National Academy of Sciences*, 117(48):30063–30070, 2020.
- [2] M. Belkin, D. Hsu, S. Ma, and S. Mandal. Reconciling modern machine-learning practice and the classical bias–variance trade-off. *Proceedings of the National Academy of Sciences*, 116(32):15849–15854, 2019.
- [3] Y. Bengio. Learning deep architectures for AI. *Foundations and trends® in Machine Learning*, 2(1):1–127, 2009.
- [4] S. Bubeck and M. Sellke. A universal law of robustness via isoperimetry. *Advances in Neural Information Processing Systems*, 34:28811–28822, 2021.
- [5] J. Devlin, M.-W. Chang, K. Lee, and K. Toutanova. BERT: Pre-training of deep bidirectional transformers for language understanding. In *Proceedings of the 2019 Conference of the North American Chapter of the Association for Computational Linguistics: Human Language Technologies, Volume 1 (Long and Short Papers)*, pages 4171–4186, 2019.
- [6] C. Fang, H. He, Q. Long, and W. J. Su. Exploring deep neural networks via layer-peeled model: Minority collapse in imbalanced training. *Proceedings of the National Academy of Sciences*, 118(43):e2103091118, 2021.
- [7] A. Fawzi, M. Balog, A. Huang, T. Hubert, B. Romera-Paredes, M. Barekatin, A. Novikov, F. J. R Ruiz, J. Schrittwieser, G. Swirszcz, et al. Discovering faster matrix multiplication algorithms with reinforcement learning. *Nature*, 610(7930):47–53, 2022.
- [8] X. Glorot and Y. Bengio. Understanding the difficulty of training deep feedforward neural networks. In *Proceedings of the Thirteenth International Conference on Artificial Intelligence and Statistics*, volume 9, pages 249–256. PMLR, 2010.
- [9] T. Hastie, R. Tibshirani, and J. H. Friedman. *The elements of statistical learning: data mining, inference, and prediction*, volume 2. Springer, 2009.
- [10] H. He and W. J. Su. The local elasticity of neural networks. In *International Conference on Learning Representations*, 2020.
- [11] K. He and J. Sun. Convolutional neural networks at constrained time cost. In *2015 IEEE Conference on Computer Vision and Pattern Recognition*, pages 5353–5360, 2015.
- [12] K. He, X. Zhang, S. Ren, and J. Sun. Deep residual learning for image recognition. In *2016 IEEE Conference on Computer Vision and Pattern Recognition*, pages 770–778, 2016.
- [13] S. Hihi and Y. Bengio. Hierarchical recurrent neural networks for long-term dependencies. In D. Touretzky, M. Mozer, and M. Hasselmo, editors, *Advances in Neural Information Processing Systems*, volume 8. MIT Press, 1995.
- [14] S. Hochreiter and J. Schmidhuber. Flat minima. *Neural Computation*, 9(1):1–42, 1997.
- [15] A. G. Howard, M. Zhu, B. Chen, D. Kalenichenko, W. Wang, T. Weyand, M. Andreetto, and H. Adam. Mobilenets: Efficient convolutional neural networks for mobile vision applications. *arXiv preprint arXiv:1704.04861*, 2017.

- [16] M. Hutson. Has artificial intelligence become alchemy? *Science*, 360(6388):478–478, 2018.
- [17] S. Ioffe and C. Szegedy. Batch normalization: Accelerating deep network training by reducing internal covariate shift. In *Proceedings of the 32nd International Conference on Machine Learning*, volume 37, pages 448–456. PMLR, 2015.
- [18] A. Jacot, F. Gabriel, and C. Hongler. Neural tangent kernel: Convergence and generalization in neural networks. *Advances in Neural Information Processing Systems*, 31, 2018.
- [19] D. P. Kingma and J. Ba. Adam: A method for stochastic optimization. In *International Conference on Learning Representations*, 2015.
- [20] A. Krizhevsky. Learning multiple layers of features from tiny images. Master’s thesis, University of Toronto, 2009.
- [21] A. Krizhevsky, I. Sutskever, and G. E. Hinton. ImageNet classification with deep convolutional neural networks. In *Advances in Neural Information Processing Systems*, volume 25, 2012.
- [22] Y. LeCun. The MNIST database of handwritten digits. <http://yann.lecun.com/exdb/mnist/>, 1998.
- [23] Y. LeCun, Y. Bengio, and G. Hinton. Deep learning. *Nature*, 521(7553):436–444, 2015.
- [24] Y. Lu, A. Zhong, Q. Li, and B. Dong. Beyond finite layer neural networks: Bridging deep architectures and numerical differential equations. In *International Conference on Machine Learning*, pages 3276–3285. PMLR, 2018.
- [25] V. Papayan, X. Han, and D. L. Donoho. Prevalence of neural collapse during the terminal phase of deep learning training. *Proceedings of the National Academy of Sciences*, 117(40):24652–24663, 2020.
- [26] J. Schmidhuber. Deep learning in neural networks: An overview. *Neural Networks*, 61:85–117, 2015.
- [27] D. Silver, A. Huang, C. J. Maddison, A. Guez, L. Sifre, G. Van Den Driessche, J. Schrittwieser, I. Antonoglou, V. Panneershelvam, M. Lanctot, et al. Mastering the game of go with deep neural networks and tree search. *Nature*, 529(7587):484–489, 2016.
- [28] K. Simonyan and A. Zisserman. Very deep convolutional networks for large-scale image recognition. In *International Conference on Learning Representations*, 2015.
- [29] R. Socher, A. Perelygin, J. Wu, J. Chuang, C. D. Manning, A. Ng, and C. Potts. Recursive deep models for semantic compositionality over a sentiment treebank. In *Proceedings of the 2013 Conference on Empirical Methods in Natural Language Processing*, pages 1631–1642, 2013.
- [30] R. K. Srivastava, K. Greff, and J. Schmidhuber. Training very deep networks. In *Advances in Neural Information Processing Systems*, volume 28, 2015.
- [31] J. P. Stevens. *Applied multivariate statistics for the social sciences*. Routledge, 2012.
- [32] W. J. Su. Neurashed: A phenomenological model for imitating deep learning training. *arXiv preprint arXiv:2112.09741*, 2021.
- [33] M. Tan and Q. Le. EfficientNet: Rethinking model scaling for convolutional neural networks. In *Proceedings of the 36th International Conference on Machine Learning*, volume 97, pages 6105–6114. PMLR, 2019.
- [34] I. Tenney, D. Das, and E. Pavlick. BERT rediscovers the classical NLP pipeline. In *Proceedings of the 57th Annual Meeting of the Association for Computational Linguistics*, pages 4593–4601, 2019.
- [35] T. Wolf, L. Debut, V. Sanh, J. Chaumond, C. Delangue, A. Moi, P. Cistac, T. Rault, R. Louf, M. Funtowicz, J. Davison, S. Shleifer, P. von Platen, C. Ma, Y. Jernite, J. Plu, C. Xu, T. Le Scao, S. Gugger, M. Drame, Q. Lhoest, and A. Rush. Transformers: State-of-the-art natural language processing. In *Proceedings of the 2020 Conference on Empirical Methods in Natural Language Processing: System Demonstrations*, pages 38–45, 2020.

- [36] H. Xiao, K. Rasul, and R. Vollgraf. Fashion-MNIST: a novel image dataset for benchmarking machine learning algorithms. *arXiv preprint arXiv:1708.07747*, 2017.
- [37] D. Yarotsky. Error bounds for approximations with deep ReLU networks. *Neural Networks*, 94:103–114, 2017.
- [38] M. D. Zeiler and R. Fergus. Visualizing and understanding convolutional networks. In *European Conference on Computer Vision*, pages 818–833, 2014.
- [39] C. Zhang, S. Bengio, and Y. Singer. Are all layers created equal? *Journal of Machine Learning Research*, 23(67):1–28, 2022.

A Experimental Details and Additional Results

In this section, we first detail the general setup for all experiments in Appendix A.1, then briefly highlight some distinctive settings for figures in the main text in Appendix A.2, and finally show some additional results in Appendix A.3. More details can be found in our code.³

A.1 General Setup

In this subsection, we briefly review the general setup that are used throughout the whole paper.

Network architecture. In our experiments, we mainly consider feedforward neural networks (FNNs). Unless otherwise stated, the corresponding hidden size is 100. For simplicity, we use neural networks with 4, 8, 20 layers as representatives for shallow, mid, and deep neural networks. By default, batch normalization [17] is inserted after fully connected layers and before the ReLU nonlinear activation functions.

Dataset. Our experiments are mainly conducted on Fashion-MNIST. Unless otherwise stated, we resize the original images to 10×10 pixels. By default, we randomly sample a total of 1000 training examples evenly distributed over the 10 classes.

Optimization methodology. In our experiments, three popular optimization methods are considered: SGD, SGD with momentum, and Adam. The weight decay is set to 5×10^{-4} , and the momentum term is set to 0.9 for SGD with momentum. The neural networks are trained for 600 epochs with a batch size of 128. The initial learning rate is annealed by a factor of 10 at 1/3 and 2/3 of the 600 epochs. As for SGD and SGD with momentum, we pick the model resulting in the best equi-separation law in the last epoch among the seven learning rates: 0.001, 0.003, 0.01, 0.03, 0.1, 0.3, and 1.0. Similarly, we pick the model resulting in the best equi-separation law in the last epoch for Adam among the five learning rates: 3×10^{-5} , 1×10^{-4} , 3×10^{-4} , 1×10^{-3} , 3×10^{-3} . Unless otherwise stated, Adam is adopted in the experiments.

A.2 Detailed Experimental Settings

In this subsection, we show detailed experimental settings for the figures in the main text.

³Our code is publicly available at <https://github.com/HornHehhf/Equi-Separation>.

Optimization. As shown in Figure 1, for FNNs with different depths, three different optimization methods are considered: SGD, SGD with momentum, and Adam.

As shown in Figure 2, we further consider the impact of the following factors on the equi-separation law: dataset, learning rate, network architecture, and class distribution.

Dataset. As shown in Figure 2, we experiment with CIFAR-10. We use the second channel of the images and resize the original images to 10×10 . Similar to Fashion-MNIST, we randomly sample a total of 1000 training examples evenly distributed over the 10 classes.

Learning rate. As shown in Figure 2, we compare the 9-layer FNNs trained using SGD with different learning rates on Fashion-MNIST.

Convolutional neural networks (CNNs). As shown in Figure 2, we experiment with two canonical CNNs, AlexNet and VGG [28]. We use the PyTorch implementation of both models.⁴ We experiment with both Fashion-MNIST and CIFAR-10, and the original images are resized to 32×32 pixels. Given that AlexNet and VGG are designed for ImageNet images with 224×224 pixels, we make some small modifications to handle images with 32×32 pixels. As for AlexNet, we change the original convolution filters to 5×5 convolution filters with padding 2. The color channel number is multiplied by 32 at the beginning. As for VGG, we change the original convolution filters to 5×5 convolution filters with padding 2, and the last average pooling layer before fully connected layers is replaced by an average pooling layer over a 1×1 pixel window. The color channel number is multiplied by 16 at the beginning.

Imbalanced data. As shown in Figure 2, we experiment with imbalanced data. Specifically, we consider 5 majority classes with 500 examples in each class, and 5 minority classes with 100 examples in each class. The law of equi-separation also emerges in neural networks trained with imbalanced Fashion-MNIST data, though its half-life is significantly larger than that in the balanced case. This might be caused by the collapse of minority classifiers as shown in [6].

Depth. As shown in Figure 3, besides Fashion-MNIST and CIFAR-10, we also consider MNIST to illustrate the optimal depth for different datasets. Similar to Fashion-MNIST, we resize the original MNIST images to 10×10 pixels, and randomly sample a total of 1000 training examples evenly distributed over the 10 classes.

As shown in Figure 4, we consider FNNs with different widths and shapes.

Width. As shown in Figure 4, we consider FNNs with three different widths. All layers have the same width in each setting. For simplicity, we consider the 8-layer FNNs trained on Fashion-MNIST.

Shape. As shown in Figure 4, we consider three different shapes of FNNs: Narrow-Wide, Wide-Narrow, and Mixed. As for Narrow-Wide, the FNNs have narrow hidden layers at the beginning, and then have wide hidden layers in the later layers. Similarly, we use Wide-Narrow to denote

⁴More details are in <https://github.com/pytorch/vision/tree/main/torchvision/models>.

FNNs that start with wide hidden layers followed by narrow hidden layers. In the case of Mixed, the FNNs have more complicated patterns of the widths of hidden layers. For simplicity, we only consider 8-layer FNNs trained on Fashion-MNIST. The corresponding widths of hidden layers for Narrow-Wide, Wide-Narrow, and Mixed we considered in our experiments are as follows: (100, 100, 100, 100, 1000, 1000, 1000), (1000, 1000, 1000, 1000, 100, 100, 100), and (100, 500, 500, 2500, 2500, 500, 500).

Out-of-sample performance. As shown in Figure 5, given 20-layer FNNs, instead of the standard training, we also consider the following two-stage frozen training procedure: 1) freeze the last 10 layers and train the first 10 layers; 2) freeze the first 10 layers and train the last 10 layers. When we conduct the frozen and standard training on CIFAR-10, we find that the our-of-sample performance of standard training (test accuracy: 23.85%) is better than that of frozen training (test accuracy: 19.67%), even though the two training procedures have similar training losses (standard: 0.0021; frozen: 0.0019) and training accuracies (standard: 100%; frozen: 100%). This is consistent with the equi-separation law: the neural networks trained using standard training have much clearer equi-separation law compared to the neural networks trained using frozen training. Specifically, the corresponding Pearson correlation coefficients for standard and frozen training are -0.997 and -0.971 , respectively.

Residual neural networks (ResNets). As shown in Figure 6, we consider three different types of ResNets: ResNets with 2-layer blocks, ResNets with 3-layer blocks, and ResNets with mixed blocks. For 3-layer blocks, the expansion rate is set to 1 instead of 4, and the original 1×1 and 3×3 convolution filters are replaced by 5×5 convolution filters. For all types of ResNets, the channel number is set to 8, and the color channel number is also multiplied by 8 at the beginning. In this part, the Fashion-MNIST images are resized to 32×32 pixels instead of 10×10 pixels.

A.3 Additional Results

In this subsection, we provide some additional results for the equi-separation law.

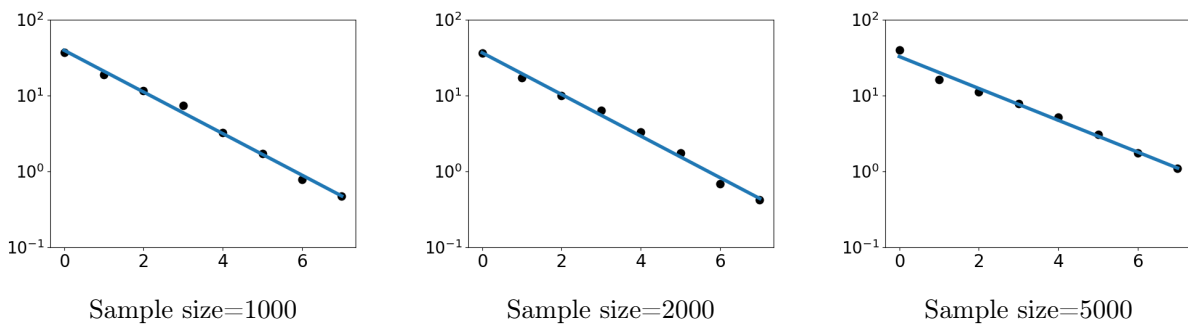


Figure 7: The impact of the sample size on the law of equi-separation.

Sample size. As shown in Figure 7, we experiment with different number of randomly sampled training examples. For each setting, we have the same number of examples for each of the 10

classes. For simplicity, we only consider the 8-layer FNNs trained on Fashion-MNIST. The law of equi-separation emerges in neural networks trained with different number of training examples, though the half-life can be larger for larger datasets due to the increased optimization difficulty.

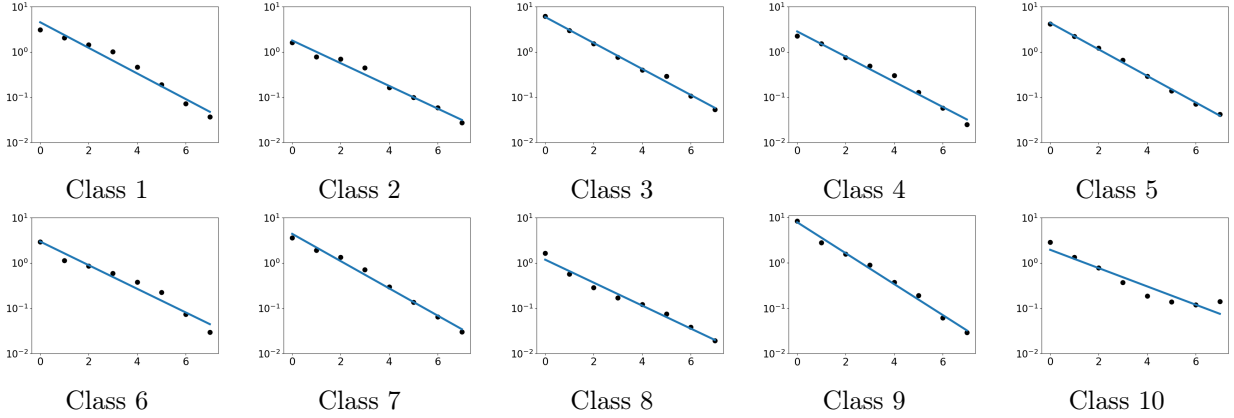


Figure 8: The law of equi-separation emerges for each class.

Class-wise data separation. As shown in Figure 8, we further consider separation fuzziness for each class, i.e., $SS_w^k SS_b^+$, where SS_w^k indicates the within-class covariance for Class k . For simplicity, we only consider the 8-layer FNNs trained on Fashion-MNIST. The equi-separation law emerges in each class. Even though the equi-separation law can be a little noisy for some classes, the noise is reduced when we consider the separation fuzziness for all classes.

Training epoch. As shown in Figure 9, we show the separability of features among layers in different training epochs. In this part, we simply consider the 20-layer FNNs trained on Fashion-MNIST. The equi-separation law doesn't emerge at the beginning, and gradually emerges during training. After that the decay ratio is decreased along the training process until the network converges.

Training dynamics. As shown in Figure 10, we consider the convergence rates of different layers (without the last-layer classifier) with respect to the relative improvement $\frac{D_{l+1}}{D_l}$ of separability of features. For simplicity, we consider the 8-layer FNNs trained on CIFAR-10 in this part. The relative improvement of bottom layers converges earlier compared to those of top layers.

Visualization. As shown in Figure 11, we visualize the features of different layers in the 8-layer FNNs trained on Fashion-MNIST. In particular, principal component analysis (PCA) is used to visualize the features in a two-dimensional plane.

Test data. As shown in Figure 12, we further show how features separate across layers in the test data. For simplicity, we only consider the 8-layer FNNs trained on Fashion-MNIST here. A fuzzy version of the equi-separation law also exists in the test data.

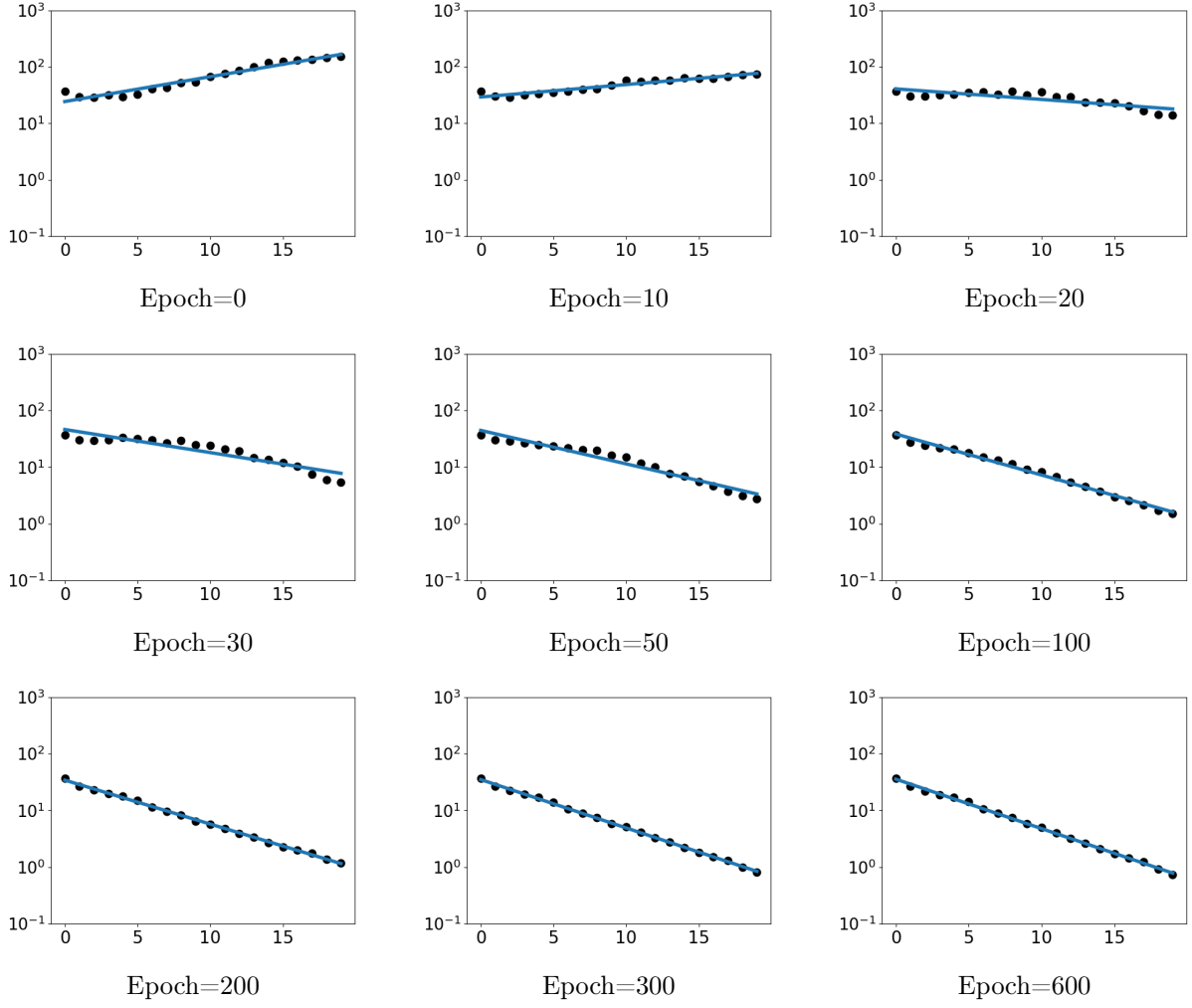


Figure 9: The impact of the training epoch on the law of equi-separation.

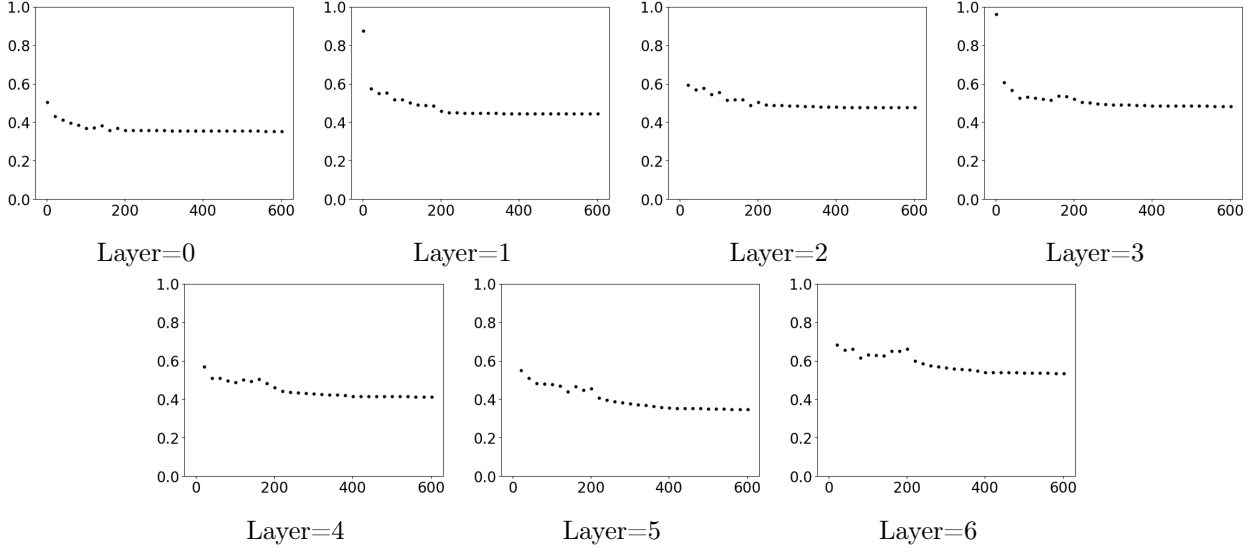


Figure 10: Convergence rates of different layers (without the last-layer classifier) with respect to the relative improvement ($\frac{D_{l+1}}{D_l}$) of separability of features.

Pretraining. As shown in Figure 13, we consider the impact of the pretraining on the equi-separation law. Specifically, we first pretrained the 20-layer FNNs on FashionMNNIST as shown in Figure 13a. After that we fix the first 10 layers of the pretrained model and train additional 5 layers (Figure 13c), which is quite different from training 15-layer FNNs from scratch (Figure 13b). At the same time, the equi-separation law also emerges in the additional 5 layers in the pretraining setting.

BERT. As shown in Figure 14, we experiment with BERT features. We use the pretrained case-sensitive BERT-base PyTorch implementation [35], and the common hyperparameters for BERT. Specifically, we fine-tuned the pretrained BERT model on a binary sentiment classification task (SST-2) [29], where we randomly sampled 500 sentences for each class. Given a sequence of token-level BERT features, two most popular approaches are used to get the sentence-level features in each layer: 1) using the features of the first token⁵ (i.e., the [CLS] token); 2) averaging the features among all tokens in the sentence.

⁵The input layer is not considered here since the inputs of the first token do not take other tokens into account.

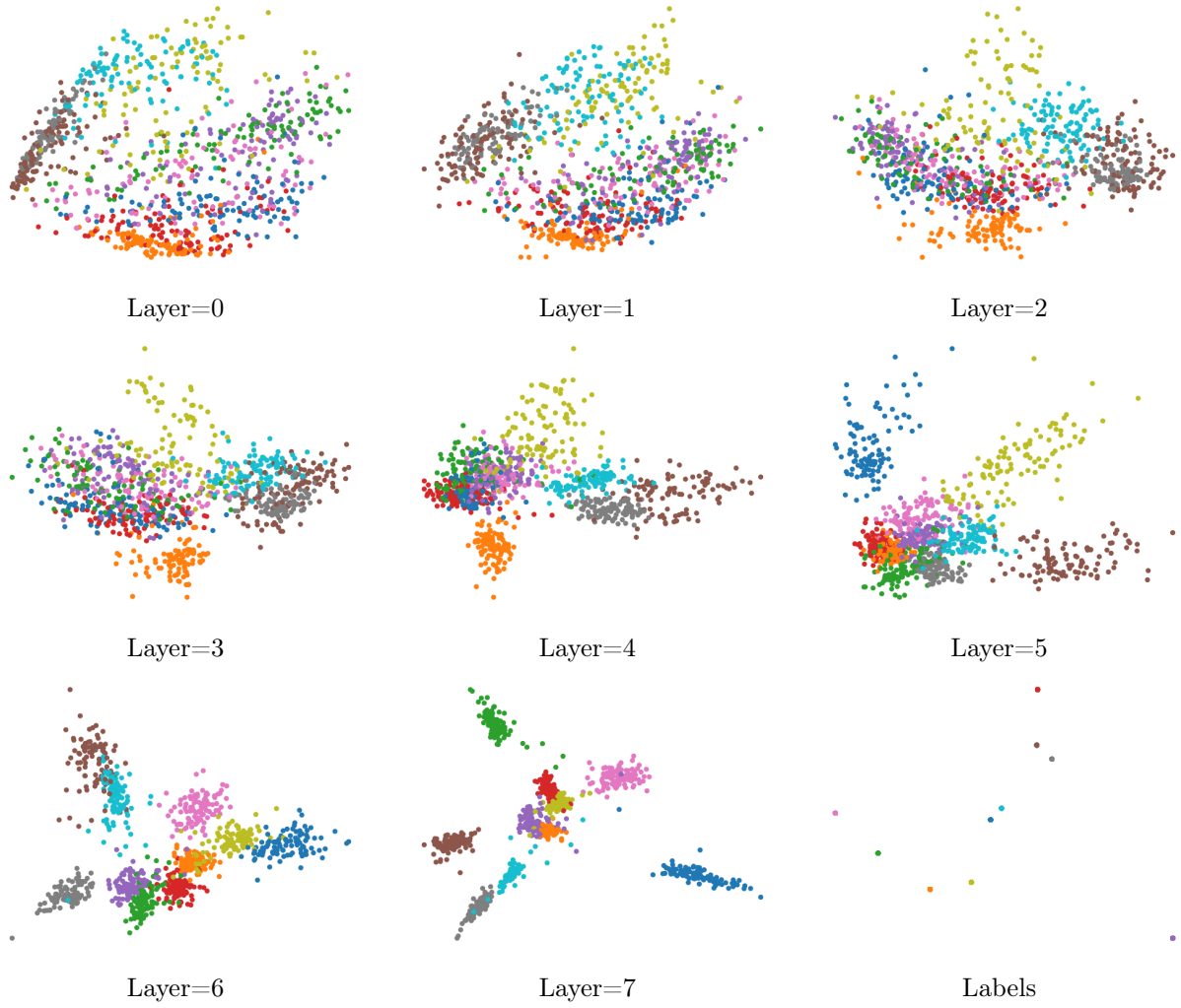


Figure 11: Visualization of intermediate data in different layers. Layer 0 corresponds to the input.

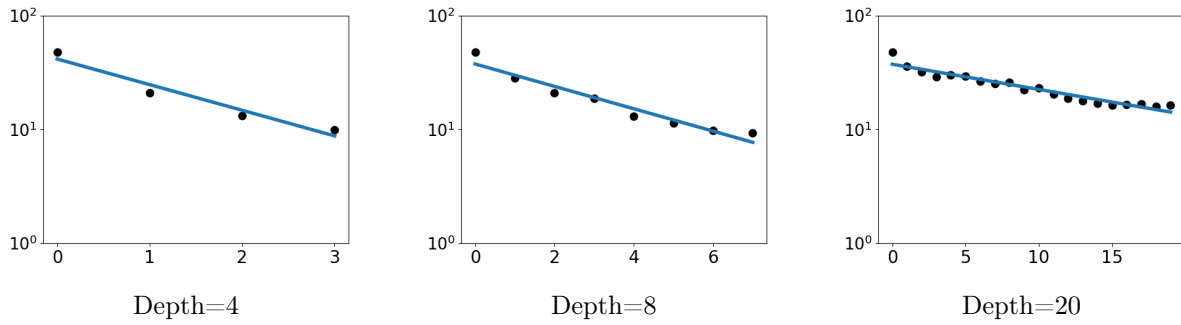


Figure 12: A fuzzy version of the equi-separation law also emerges in the test data.

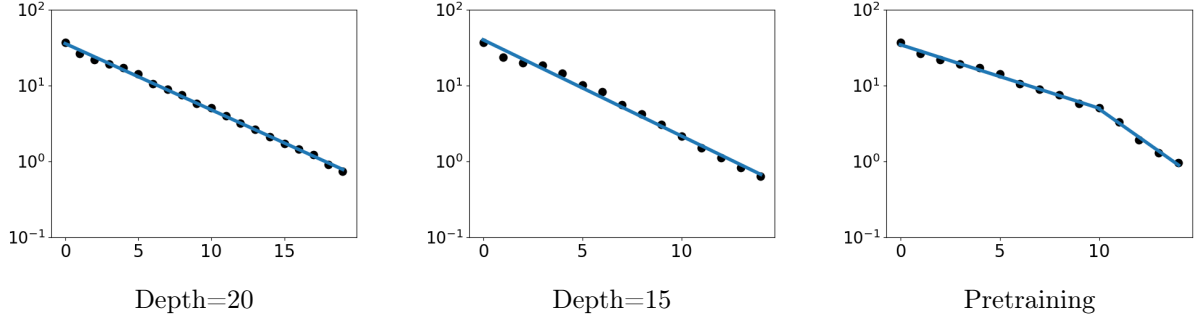


Figure 13: The impact of pretraining on the equi-separation law. We first pretrained the 20-layer FNNs as shown in Figure 13a. After that we fix the first 10 layers of the pretrained model and train additional 5 layers (Figure 13c), which is quite different from training the 15-layer neural networks from scratch (Figure 13b).

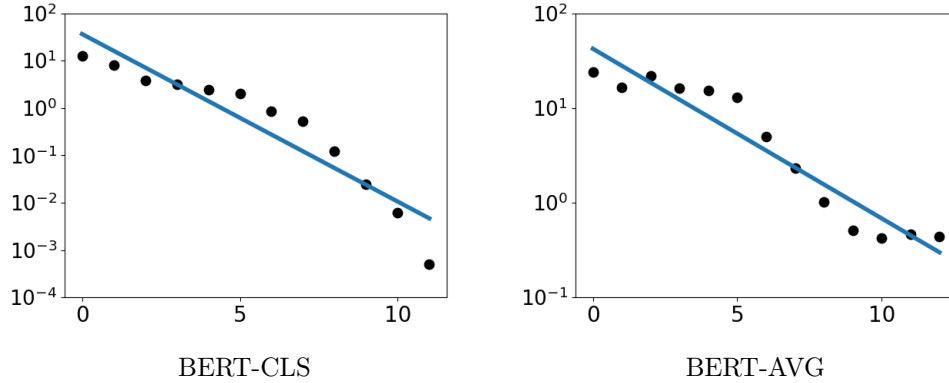


Figure 14: The equi-separation law does not exist in BERT features. Given a sequence of token-level BERT features, two most popular approaches are used to get the sentence-level features in each layer: 1) using the features of the first token (i.e., the [CLS] token); 2) averaging the features among all tokens in the sentence (denoted as BERT-AVG).